Advances in Nuclear Fuel Management III (ANFM 2003)
Hilton Head Island, South Carolina, USA, October 5-8, 2003, on CD-ROM, American Nuclear Society, LaGrange Park, IL (2003)

BENCHMARK OF SIMULATE-3K AGAINST THE FRIGG LOOP STABILITY EXPERIMENTS

Gerardo M. Grandi & Jeffrey A. Borkowski
Studsvik Scandpower, Inc.
504 Shoup Ave., Suite 201, Idaho Falls, ID 83402 U.S.A
gerardo@soa.com ; jeff@soa.com

Keywords: BWR, stability, coupled codes, validation

ABSTRACT

SIMULATE-3K is used by many utilities for the prediction and analysis of BWR stability events. In recent years, several enhancements of the SIMULATE-3K channel and vessel thermal-hydraulic model have been made. This paper summarizes the status of the SIMULATE-3K core thermal-hydraulic model and presents results of the validation against the OF64 test section experiments performed in the Frigg loop. The results comprise comparisons of channel pressure drops, void measurements, and stability limits.

1. INTRODUCTION

SIMULATE-3K (S3K)[1] is a transient code with a 3D core model. It is suitable for transient analysis that requires a detailed model of core. S3K is widely used by utilities for the analysis and prediction of BWR stability[2-4]. For stability calculations, it is important to have a core model which calculates the detailed flow, pressure drop and void conditions in each fuel assembly. Furthermore, an accurate prediction of the flow inertia, pressure drops and driving forces (pump head, elevation heads and irreversible losses) in the recirculation loop is also required.

Figure 1 shows a simplified scheme of the Frigg loop with the OF64 test section. The OF64 test section was designed as a full scale simulation of an 8x8 rod fuel assembly. Experiments were performed in 1969 in the Frigg loop on axial void distribution, single and two-phase pressure drops and hydraulic characteristics (stability limits) of different fuel assemblies. The measurements included a wide range of operating conditions such as pressure, power, inlet subcooling, inlet throttling, and pump speed. The purpose of this paper is to present the results of the validation of S3K against the above mentioned experiments.

The OF64 test section was simulated using the S3K core channel model. The balance of the experimental loop was simulated using the BWR vessel models available in S3K. The channel thermal hydraulic model was presented in Ref. 5. The BWR vessel model is discussed in Ref. 3. The status of the channel thermal hydraulic model will be discussed in Section 2. Section 3 presents the comparison of the pressure drop, void measurements, and stability limits predicted by S3K with the experimental data. Conclusions are drawn in Section 4.

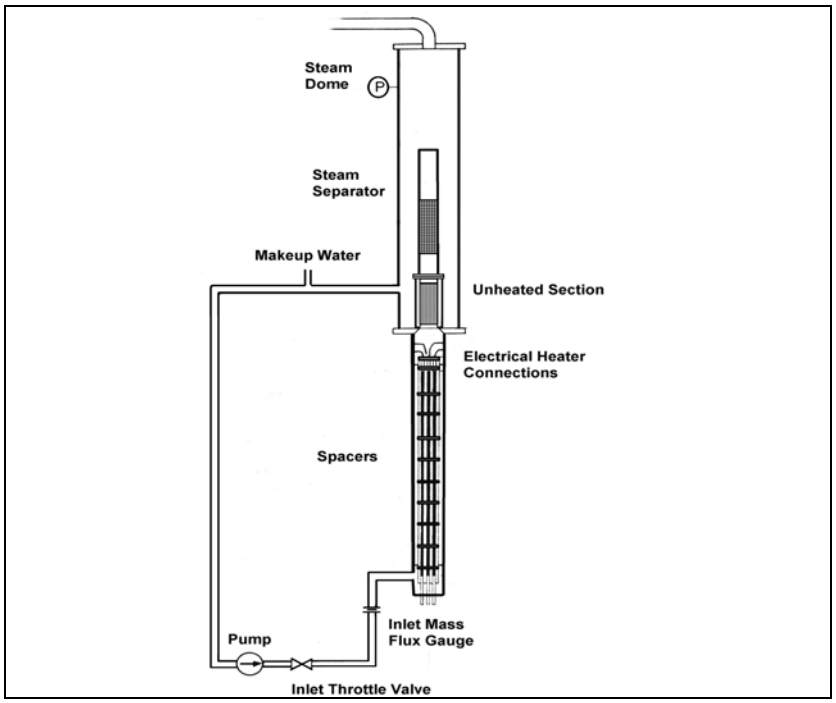

Fig. 1 Frigg Loop with OF64 Test Section.

2. CHANNEL HYDRAULIC MODEL

In S3K, the core is represented with one thermal-hydraulic channel per fuel bundle with no cross flow. The hydraulic model uses a five-equation model, vapor and liquid mass conservation, vapor and liquid energy conservation and mixture momentum conservation. The area-averaged form of the conservation equations employed in S3K is similar to that appearing in the literature. The hydraulic primitive variable set is comprised of phasic mass fluxes G_v and G_l, phasic enthalpies h_v and h_l, pressure P, and void fraction α. In addition to the conservation equations, closure relationships exist for each phasic density, defined as a function of the pressure and phasic enthalpy. It is important to mention that water properties are evaluated at the core exit pressure. The general drift formulation for the void fraction completes the set of equations to be solved. The concentration parameter and the void-weighted drift velocity are calculated using the EPRI correlations[6].

All primitive variables in the S3K channel hydraulics are defined on a consistent edge-centered mesh. The spatial discretization is obtained by performing volume integration from lower to upper mesh edge, thereby preserving node integral quantities appearing in the temporal derivative and (non-gradient) source terms. The time discretized form of the conservation equations is obtained by backward time integration.

3. RESULTS

The next three subsections compare the S3K results against pressure drop measurements[7], void measurements[8], and stability limits[9], respectively.

3.1 Pressure drop measurements

Simulations required models only for the test section. Core exit pressure, inlet throttling, inlet subcooling, heating power in the rod cluster, and mass flux in the test section were the boundary conditions for these calculations. The mass fluxes range from 500 kg/m^2/s to 2000 kg/m^2/s; the heating powers range from 1978 kW to 5090 kW and the inlet subcooling is between 7 C and 38 C. The average pressure in the loop in this set of experiments is 6.8 MPa. Table 1 summarizes the conditions for the 25 runs chosen to compare the two-phase pressure drop distributions. The two phase friction multiplier was computed using the Chisholm correlation[10].

Table 1 Two-phase pressure drop measurements**.**

Run no	Pressure	Mass Flux	Power	Inlet Subcooling	Measured Pressure Drop	Calculated Pressure Drop	Difference
	[bar]	[kg/m^2/s]	[kW]	[C]	[Kpa]	[Kpa]	%
704017	67.5	490	1978	7.2	28	28	-0.9
704016	67.7	738	1978	7.5	37	37	0.3
704015	67.8	1257	1978	8.7	59	57	-3.5
704025	66.7	2540	3509	8.9	144	156	8.3
704020	67.9	741	3517	6.9	45	43	-3.0
704019	67.7	742	3517	7.0	45	43	-2.9
704021	67.5	1246	3517	8.1	69	69	-1.0
704053	67.2	1254	3517	7.5	71	70	-0.4
704054	67.2	758	5090	5.5	55	53	-3.8
704029	67.2	1257	5090	7.4	84	83	-1.0
704027	67.6	2008	5090	7.5	133	138	4.0
704026	67.3	2549	5090	8.3	183	164	-10.3
704031	67.1	503	1978	21.4	30	29	-2.5
704030	67.2	746	1978	23.0	38	37	-2.2
704032	67.9	500	3517	21.0	33	31	-4.9
704033	67.5	747	3517	22.0	43	41	-3.8
704035	67.7	1253	3517	22.4	63	61	-2.8
704039	66.7	1999	3527	23.6	96	97	1.2
704034	67.9	744	5090	20.8	50	47	-5.9
704038	67.4	1243	5090	22.6	74	71	-3.7
704037	67.5	1245	5090	22.3	74	71	-3.2
704040	67.4	2003	5090	22.8	110	112	1.4
704043	67.2	909	1978	37.7	44	42	-3.3
704041	67.4	1228	3527	37.0	57	56	-2.1
704042	67.5	1219	5090	36.3	66	63	-4.1

Figure 2 compares the experimental and numerical results.

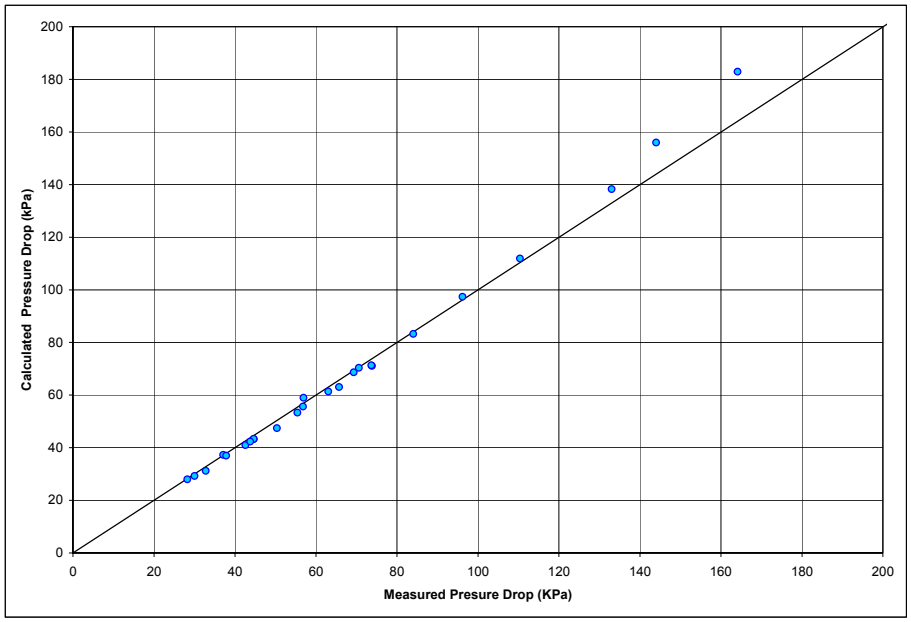

Fig. 2 Comparison of pressure drop measurements.

Figures 3 and 4 show the pressure drop distribution for two runs with similar power and flow conditions (power 3517 kW, mass flux 1253 kg/m^2/s) but different inlet subcooling, namely: run 704053 (inlet subcooling 7.5 C) and run 704035 (inlet subcooling 22.4 C)

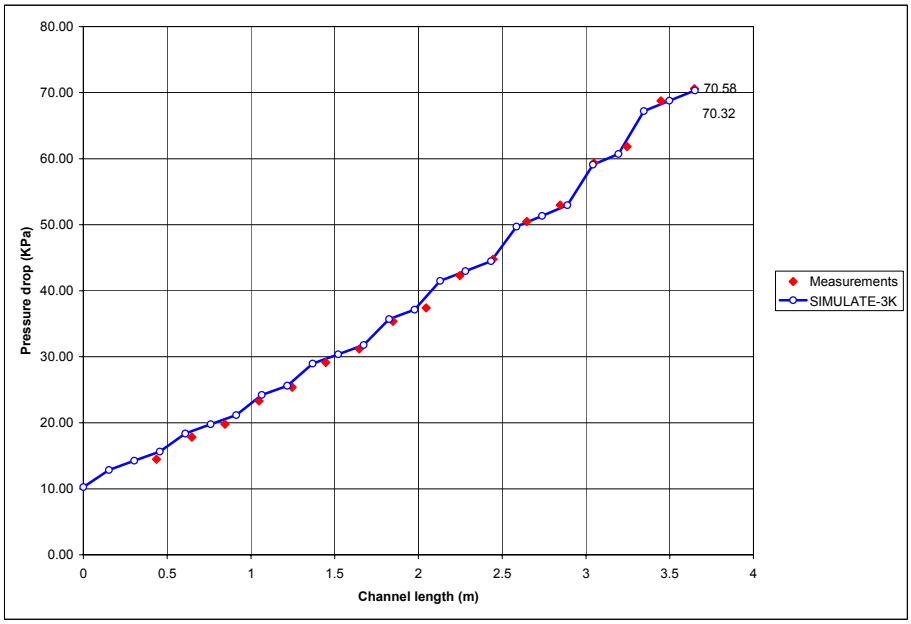

Fig. 3 Pressure drop for subcooling 7.5 C.

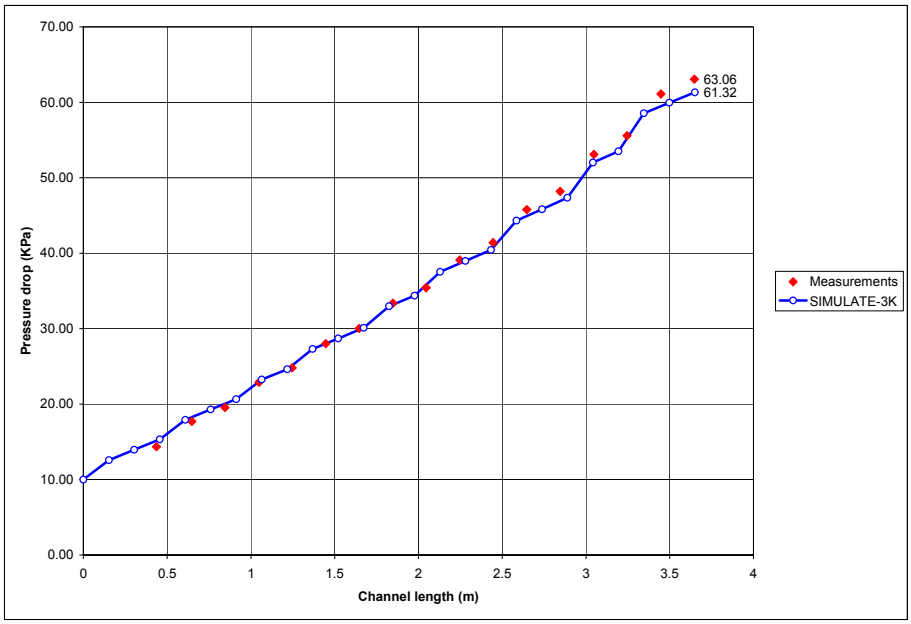

Fig. 4 Pressure drop case for subcooling = 22.4 C.

The results show good agreement with the measurements. The average bias in the pressure drop calculations is approximately 2% and the standard deviation 3.5%.

3.2 Void measurements

The boundary conditions applied in the simulations are the same as the ones applied in the simulation of the pressure drop measurements (i.e. core exit pressure, inlet throttling, inlet subcooling, heating power in the rod cluster, and mass flux in the test section). Table 2 summarizes the experimental conditions for the 30 runs used for the comparison against the void measurements. The mass fluxes range from 500 kg/m^2/s to 2000 kg/m^2/s; the average heat fluxes range from 22 W/cm^2 to 57.1 W/cm^2 and the inlet subcooling is between 9 C to 38 C. Figure 5 compares the experimental and numerical results of the 30 runs.

Table 2 Void measurements. Conditions for the selected runs.

Run no	P	G	Q	Subc
	[bar]	[kg/m^2/s]	[kW]	[C]
713001	67.8	1259	1978	9.8
713002	67.7	737	1978	9.9
713003	67.5	496	1978	9.7
713004	67.7	494	3517	8.9
713006	67.9	741	3517	9.5
713007	67.4	1250	3517	9.6
713008	67.2	1247	3507	9.1
713009	67.3	1248	3507	9.1
713010	67.2	2006	3517	9.7
713011	66.7	2479	3517	9.7
713012	67.3	2477	5079	9.1
713013	67.6	1997	5090	9.0
713014	68.2	1258	5090	9.3
713015	67.2	1260	5090	9.6
713016	67.2	754	1978	24.5
713017	67.1	507	1978	24.8
713018	67.9	507	3517	25.0
713019	67.5	750	3517	24.6
713020	67.9	746	5090	24.2
713021	67.7	1258	3517	24.0
713022	67.4	1251	3517	23.7
713023	67.5	1244	5090	24.7
713024	67.4	1245	5079	24.7
713025	66.7	2000	3517	24.8
713026	67.4	2004	5090	24.4
713027	67.4	1220	3527	38.6
713028	67.5	1220	5090	38.3
713029	67.2	904	1988	38.4
713039	67.2	1249	3517	9.1
713040	67.2	759	5090	8.9

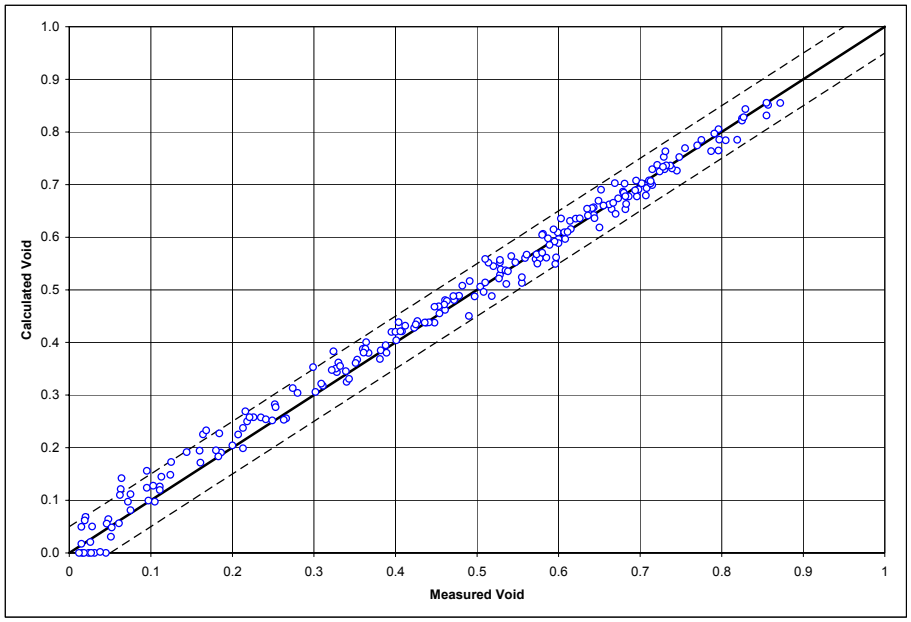

Fig. 5 Comparison of calculated and measured void fractions.

Figures 6 and 7 compare the void profiles for two runs with similar mass flux and heating power (mass flux 1258 kg/m^2/s, power 3514 kW), but different inlet subcooling, namely: run 713021 (subcooling 24.0 C) and run 713009 (subcooling 9.1 C).

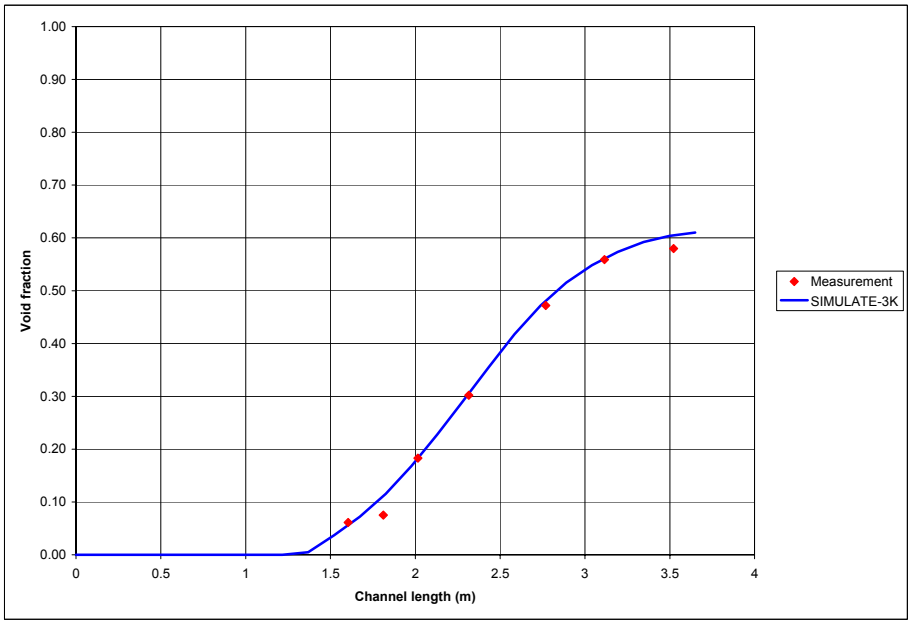

Fig. 6 Void profile for subcooling 24.0 C.

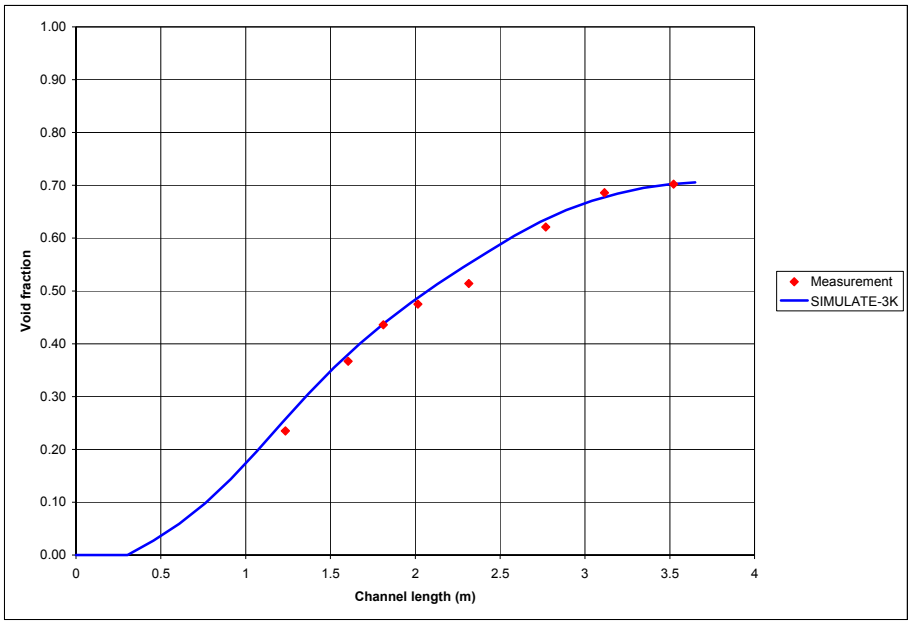

Fig. 7 Void profile for subcooling.9.1 C.

The results show good agreement with the measurements. The average bias is 0.007 and the standard deviation 0.022.

3.3 Stability limits

The simulations were performed using the complete model for the experimental loop (i.e. both the test section and the recirculation loop were explicitly modeled). The heating power in the test section, the water level, the pump speed, the steam drum pressure, and inlet subcooling were set as boundary conditions for the calculations.

The initial total flow in the loop was calculated by S3K. Figures 8 and 9 show the capability of S3K to compute the steady state flow for a wide range of operating conditions. The experimental conditions are:

- pressure 6.8 MPa,
- inlet subcooling 9 C, and 19 C,
- inlet throttling 22 v.h., and 57 v.h.,
- pump speed 500 rpm, 1000 rpm, and 1300 rpm.

Note that there is good agreement between the steady state mass fluxes calculated by S3K and the measured ones.

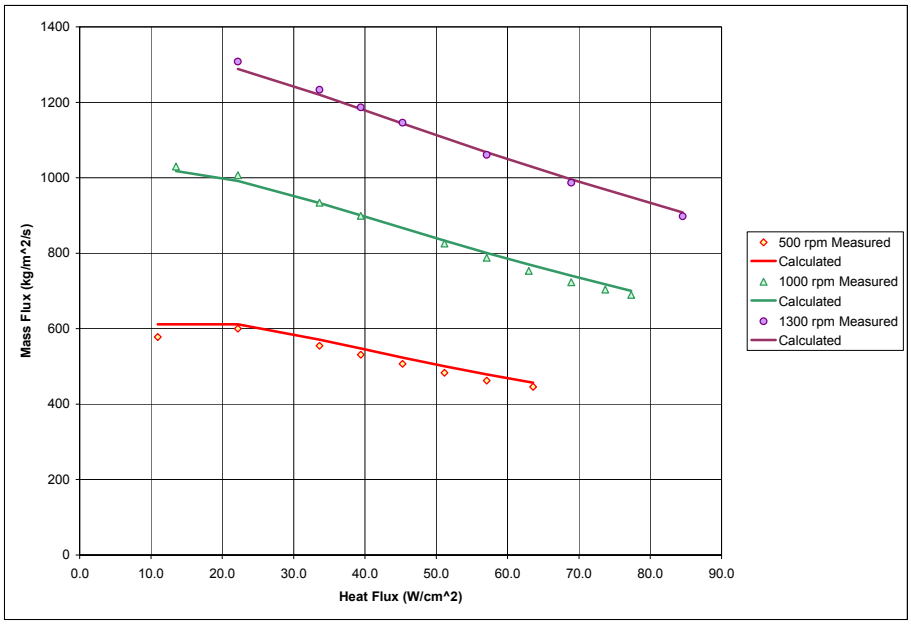

Fig. 8 Mass flux vs. heat flux. Throttling 57 v.h. , Subcooling ~ 9 C.

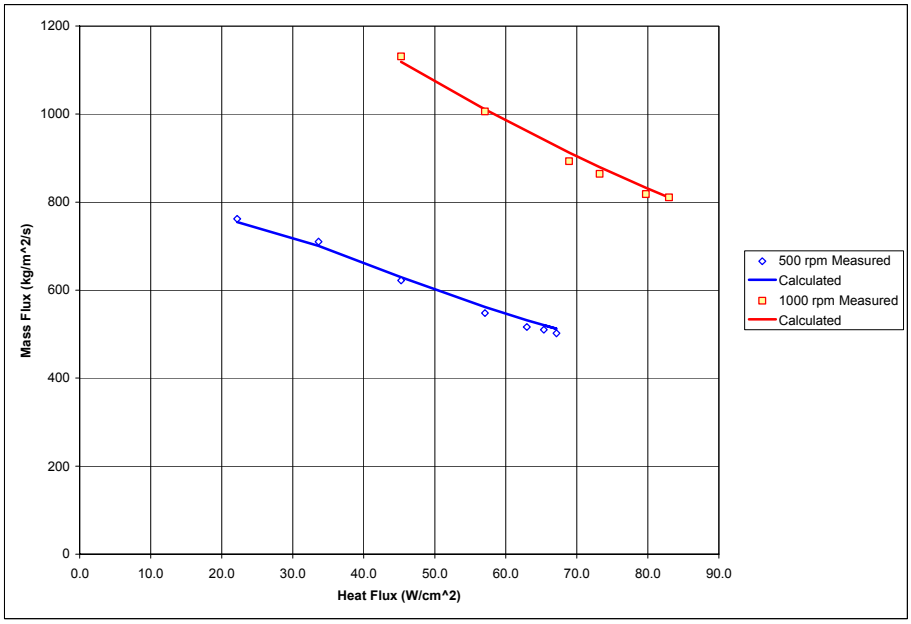

Fig. 9 Mass flux vs. heat flux. Throttling 22 v.h. , Subc. ~ 19 C.

The stability limits were computed as follows. The heating power in the rod cluster was initialized at 500 kW to 1000 kW lower than the measured instability threshold. During the transient, the power was increased stepwise 50 kW at intervals of 15 seconds. Figure 10 shows the power and inlet flow rate versus time for the run 702001-008 (pressure 6.82 MPa, pump speed 500 rpm, inlet throttling 22 v. h. and inlet subcooling 18.9 C).

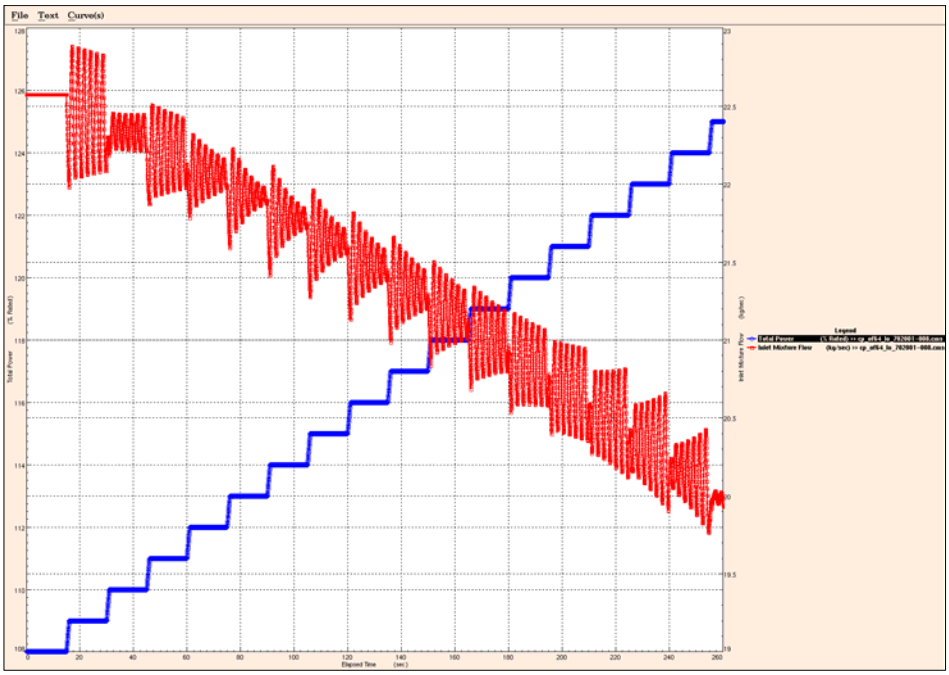

Fig. 10 Experiment 702001-008: Power and flow vs. time.

The test section inlet flow was used to determine the decay ratio of the system after each power increase. Figure 11 shows the decay ratio as function of the heating power. The average mass flux for each time interval was also calculated. The instability threshold can be easily estimated from Figure 11. Note that the calculated instability threshold (6022 kW) agrees very well with the measured value 5989 kW) for the run 702001-008. The procedure was repeated for the different experimental runs. The results are summarized in Table 3.

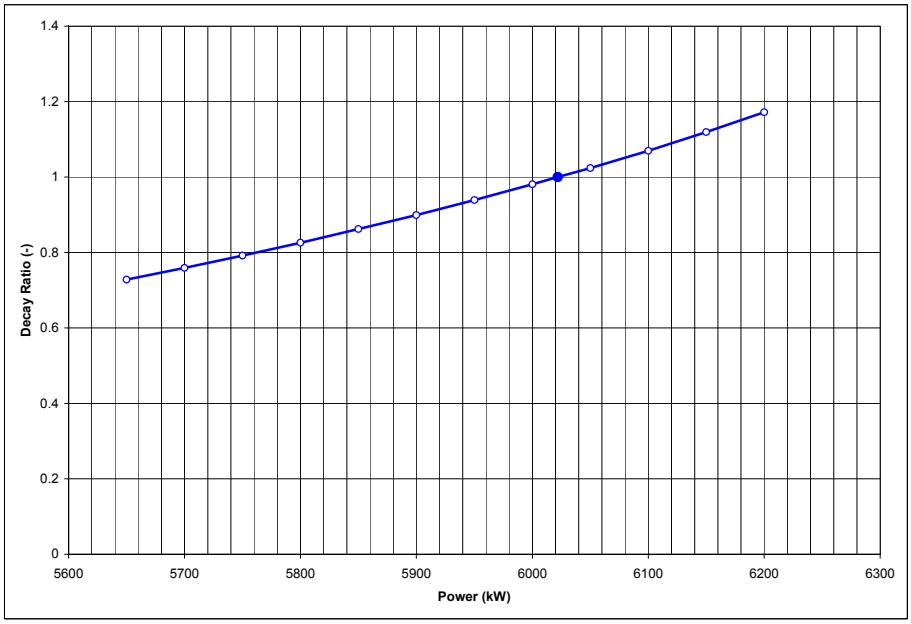

Fig. 11 Experiment 702001-008. Decay ratio vs. power.

Table 3 Power and mass flux at the instability threshold.

					Measured		Calculated		Error %	
Run no	P	SUBC	KLTP	SPEED	G	Q	G	Q	G	Q
	MPa	[C]	[v.h.]	[rpm]	[kg/m^2/s]	[kW]	[kg/m^2/s]	[kW]	%	%
702061-064	2.9	19.2	22.0	500.0	534	3517	533	3149	-0.2	-10.5
702077-081	2.9	19.2	57.2	500.0	407	3986	449	3477	10.3	-12.8
702065-069	2.9	19.2	22.0	1000.0	749	4699	811	4334	8.3	-7.8
702082-085	2.9	19.2	51.4	1000.0	616	5343	628	5290	1.9	-1.0
702070-076	2.9	19.2	22.0	1300.0	949	5914	980	5431	3.3	-8.2
702087-101	2.9	19.2	49.9	1300.0	797	6276	819	6020	2.8	-4.1
702057-060	3.9	19.0	22.0	500.0	502	4038	520	3894	3.6	-3.6
702052-056	3.9	19.0	22.0	1000.0	749	5626	808	5261	7.9	-6.5
702089-096	3.9	19.0	51.4	1000.0	613	6362	656	6009	7.0	-5.5
702026-030	4.8	9.0	22.0	500.0	463	4773	485	4598	4.8	-3.7
702040-043	4.8	9.0	22.0	1000.0	681	6682	693	6615	1.8	-1.0
702031-034	4.8	18.5	22.0	500.0	494	4689	507	4643	2.6	-1.0
702044-047	4.8	18.5	22.0	1000.0	761	6404	781	6223	2.6	-2.8
702035-039	4.8	28.3	22.0	500.0	517	5027	523	4741	1.2	-5.7
702048-051	4.8	28.3	22.0	1000.0	818	6897	803	6621	-1.8	-4.0
702015-019	5.8	18.9	22.0	500.0	500	5269	503	5289	0.6	0.4
								Average	3.3	-4.5
								Std. Dev	3.4	3.8

Figure 12 compares the power at the instability threshold (critical power) against the measured values. Figure 13 compares the calculated and measured mass fluxes at the instability threshold, i.e. the average mass flux when the power is the critical power.

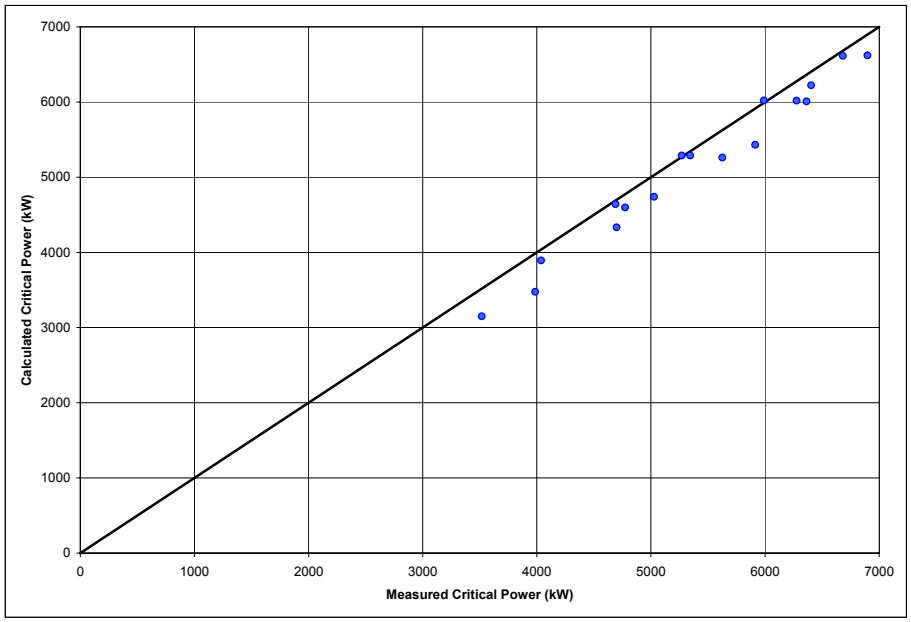

Fig. 12 Comparison of power at the instability threshold.

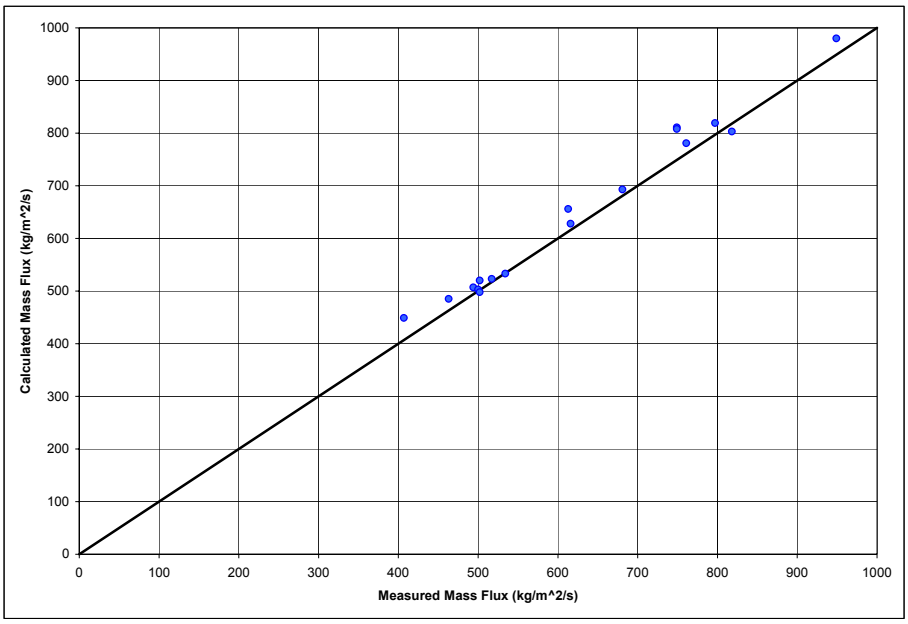

Fig. 13 Comparison of mass flux at the instability threshold.

There is good agreement between the calculations and the experimental results. The bias in the predicted critical power is -4.5% and the standard deviation 3.8%. The bias in the predicted critical mass flux is +3.3% and the standard deviation 3.4%.

The influence of the system pressure and the inlet subcooling are discussed in what follows. Five runs at 500 rpm and three runs at 1000 rpm pump speed, inlet throttling 22 v.h., and inlet subcooling at approximately 19 C were selected to study how the instability threshold depends on pressure. The data for the runs is given in Table 4. The calculated instability thresholds for all runs are compared with the measured ones in Figures 14 and 15.

Table 4 Power and mass flux at the instability threshold. Influence of the pressure.

					Measured		Calculated	
Run no	P	Subc	KLTP	Speed	G	Q	G	Q
	Mpa	[C]	[v.h.]	[rpm]	[kg/m^2/s]	[kW]	[kg/m^2/s]	[kW]
702061-064	2.9	19.2	22.0	500.0	534	3517	533	3149
702057-060	3.9	19.0	22.0	500.0	502	4048	520	3894
702031-034	4.8	18.5	22.0	500.0	494	4689	507	4643
702015-019	5.8	18.9	22.0	500.0	500	5269	503	5289
702001-008	6.8	18.9	22.0	500.0	502	5989	498	6022
702065-069	2.9	19.2	22.0	1000.0	749	4699	811	4334
702052-056	3.9	19.0	22.0	1000.0	749	5628	808	5261
702044-047	4.8	18.5	22.0	1000.0	761	6404	781	6223

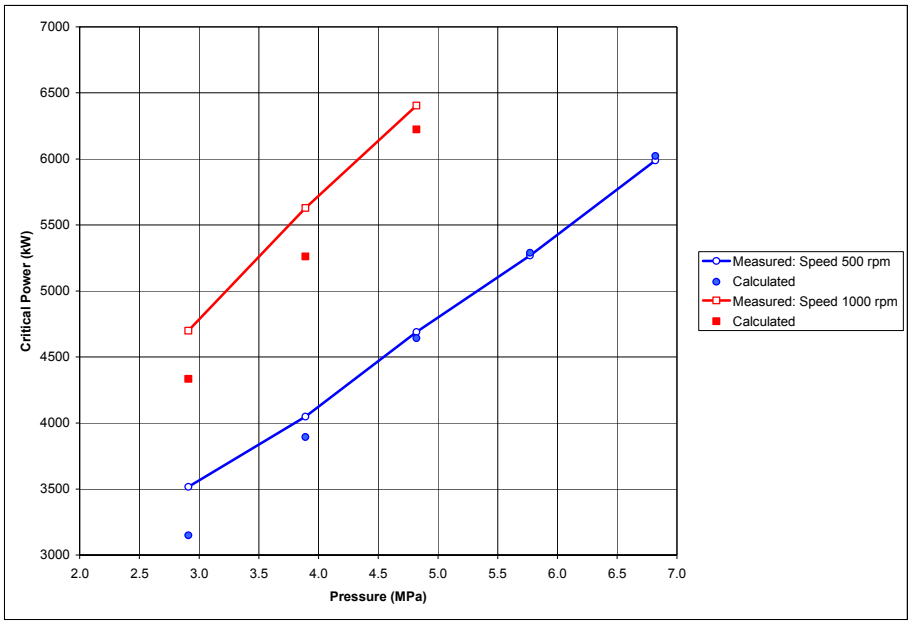

Fig. 14 Comparison of mass flux at the instability threshold.

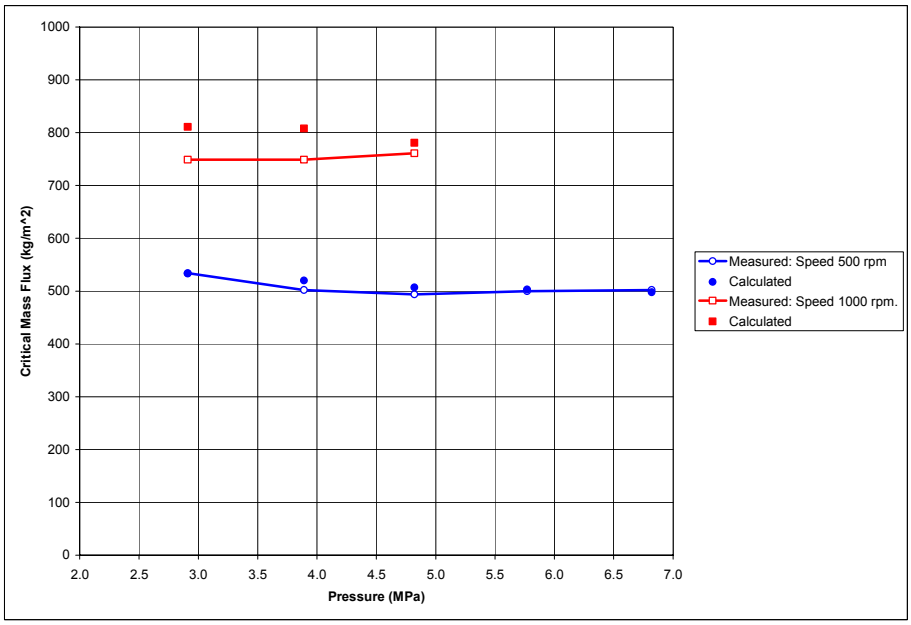

Fig. 15 Mass flux at the instability threshold. Influence of the pressure.

The error in the critical power estimated by S3K at typical BWR operating conditions (6.8 MPa) is very small. The experimental results show that mass flux at the critical power is almost a constant for a given pump speed (i.e. it does not depend on the system pressure), and S3K shows the same behavior.

Table 5 shows the 6 runs used to study the influence of the inlet subcooling on the instability threshold.

Table 5 Power and mass flux at the instability threshold. Influence of inlet subcooling.

					Measured		Calculated	
Run no	P	Subc	KLTP	Speed	G	Q	G	Q
	Mpa	[C]	[v.h.]	[rpm]	[kg/m^2/s]	[kW]	[kg/m^2/s]	[kW]
702026-030	4.8	9.0	22.0	500.0	463	4773	485	4598
702031-034	4.8	18.5	22.0	500.0	494	4689	507	4643
702035-039	4.8	28.3	22.0	500.0	517	5027	523	4741
702040-043	4.8	9.0	22.0	1000.0	681	6682	693	6615
702044-047	4.8	18.5	22.0	1000.0	761	6404	781	6223
702048-051	4.8	28.3	22.0	1000.0	818	6897	803	6621

Table 5 and Figure 16 compare the calculated and measured critical power. The agreement is quite good. Note that the measured critical power has a minimum when the subcooling is approximately 19 C. This tendency is predicted by S3K.

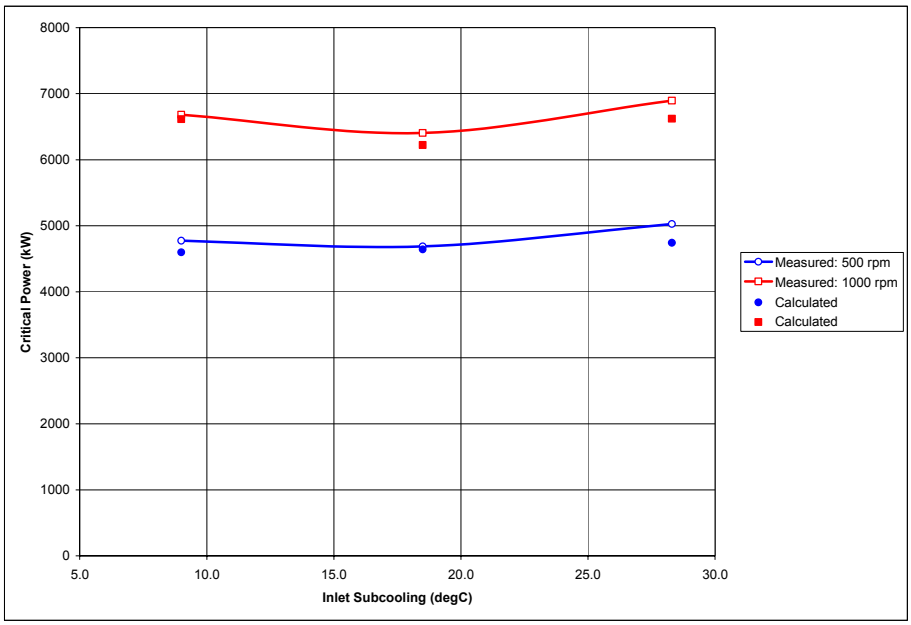

Fig. 16 Power at the instability threshold. Influence of the inlet subcooling.

4. CONCLUSIONS

The SIMULATE-3K two-phase pressure drops show good agreement with the measurements. The average bias in the pressure drop calculations is approximately 2% and the standard deviation 3.5%. The comparison of the void measurements is also in good agreement. The average bias is 0.007 and the standard deviation 0.022.

SIMULATE-3K is capable of predicting the instability threshold for a wide range of operating conditions. The bias is -4.5% and the standard deviation +3.8%. The instability threshold at BWR nominal pressure condition is very good (+0.8% difference).

The experimental results show that the mass flux at the instability threshold is independent of the system pressure (for a given pump speed, core inlet subcooling and throttling). This behavior is also predicted by S3K. The dependency of the instability threshold with the system pressure and inlet subcooling is good.

SIMULATE-3K is a best-estimate code used for stability analysis of BWR. Results presented in this paper are part of the qualification of the S3K thermal-hydraulic models for BWR stability analysis.

REFERENCES

1. J. BORKOWSKI, J. RHODES III, P. ESSER, K. SMITH, "A Three-Dimensional Transient Analysis Capability for SIMULATE-3," *Trans. Am. Nuc. Soc.*, **71**, 456, (1994).

2. J. BORKOWSKI, K. SMITH, D. HAGRMAN, D. KROPACZEK, J. RHODES III, P. ESSER, "SIMULATE-3K Simulations of the Ringhals-1 BWR Stability Measurements," *Proceeding of International Conference on the Physics of the Reactors Physor 1996*, Mito, Ibaraki, Japan, September 16-20, (1996).

3. G. M. GRANDI, K. S. SMITH, "BWR Stability Analysis with SIMULATE-3K," *Proceedings PHYSOR 2002*, Seoul, Korea, October 2-10, (2002).

4. M. KRUNERS, "Analysis of Instability Event in Oskarshamn-3, Feb. 8, 1998, with SIMULATE-3K," SKI Report 98:42, Statens Kärnkraftinspektion, SE-10658, Stockholm, (1998).

5. D. J. KROPACZEK, K. S. SMITH, J. A. BORKOWSKI, "A Fully Implicit Five Equation Channel Hydraulics Model for SIMULATE-3K," *Proceedings Joint Int. Conf. on Mathematical Methods and Supercomputing for Nuclear Applications*, Saratoga Springs, Vol. 1. 1401, (1997).

6. G. S. LELLOUCHE, B. A. ZOLOTAR, "Mechanistic Model for Predicting Two-Phas Void Friction for Water in Vertical Tubes, Channels, and Rod Bundles, EPRI NP-2246-SR, November (1982).

7. O. GELIUS AND G. MANOV, "OF-64 Results of Pressure Drop Measurements", FRIGG PM-71, Asea Atom, May (1970).

8. O. NYLUND R. EKLUND, "OF-64 Results of Void Measurements", FRIGG PM-69, Asea Atom, February (1970).

9. R. EKLUND, O. NYLUND AND A. JENSEN, "OF-64 Hydraulic Characteristics and Stability Limits", FRIGG PM-68, Asea Atom, February (1970).

10. D. CHISHOLM, "Pressure Gradients Due to Friction During the Flow of Evaporating Two-Phase Mixture in Smooth Tubes and Channels," *Int. J. Heat Mass Transfer*, **16**, (1973).